Biophysical characterization of the association of histones with single-stranded DNA

Ying Wang [a], Luis van Merwyk [a], Katja Tönsing [a], Volker Walhorn [a], Dario Anselmetti [a], Xavier Fernàndez-Busquets [b,c,d,*]

[a] Experimental Biophysics and Applied Nanoscience, Faculty of Physics, Bielefeld University, Bielefeld 33615, Germany

[b] Nanomalaria Group, Institute for Bioengineering of Catalonia (IBEC), The Barcelona Institute of Science and Technology, Baldiri Reixac 10-12, Barcelona 08028, Spain

[c] Barcelona Institute for Global Health (ISGlobal), Barcelona Center for International Health Research (CRESIB, Hospital Clínic-Universitat de Barcelona), Rosselló 149-153, Barcelona 08036, Spain

[d] Nanoscience and Nanotechnology Institute (IN2UB), University of Barcelona, Martí i Franquès 1, Barcelona 08028, Spain

* Corresponding author.
E-mail address: xfernandez_busquets@ub.edu

ABSTRACT

Background: Despite the profound current knowledge of the architecture and dynamics of nucleosomes, little is known about the structures generated by the interaction of histones with single-stranded DNA (ssDNA), which is widely present during replication and transcription.

Methods: Non-denaturing gel electrophoresis, transmission electron microscopy, atomic force microscopy, magnetic tweezers.

Results: Histones have a high affinity for ssDNA at physiological salt concentrations, with an apparent binding constant similar to that calculated for their association with double-stranded DNA (dsDNA). The length of DNA (number of nucleotides in ssDNA or base pairs in dsDNA) associated with a fixed core histone mass is the same for both ssDNA and dsDNA. Whereas histone-ssDNA complexes show a high tendency to aggregate in 0.2 M NaCl, at lower ionic strength nucleosome-like structures are formed. Core histones are able to protect ssDNA from digestion by micrococcal nuclease, and a shortening of ssDNA occurs upon its interaction with histones. The purified (+) strand of a cloned DNA fragment of nucleosomal origin has a higher affinity for histones than the purified complementary (–) strand.

Conclusions: At physiological ionic strength histones have high affinity for ssDNA, possibly associating with it into nucleosome-like structures.

General Significance: In the cell nucleus histones may spontaneously interact with ssDNA to facilitate their participation in the replication and transcription of chromatin.

Keywords: single-stranded DNA; histones; nucleosome; magnetic tweezers; electrophoresis; force spectroscopy

1. Introduction

Nucleosomes are present even in chromatin regions where replication and transcription are taking place [1,2]. In spite of the detailed knowledge of its three-dimensional structure [3], the nucleosome is no longer viewed as a single static entity: rather, it is a family of particles varying in their structural and dynamic properties, leading to different functionalities [4]. It seems clear that the precise positioning of nucleosomes on particular DNA sequences is directly related to the regulation of chromatin activity (reviewed in [5,6]), but the molecular processes that allow the elongation of DNA and RNA chains in eukaryotic genes containing nucleosomes are not completely elucidated yet. The linker histones H1 and H5 are partially displaced from active genes [7], but results coming from several laboratories have indicated different fates for core histones during transcription, suggesting various mechanisms for transcription elongation [2,8]. The remarkable conformational flexibility of nucleosome cores detected using various physicochemical techniques [1,9,10] could facilitate the passage of RNA polymerase without modification of histone composition. However, during transcription the DNA template is extensively distorted as it passes through the narrow active center of RNA polymerase [11], which makes it unlikely for transcription to occur without drastic nucleosomal disruption. Indeed, *in vitro* transcription assays with nucleosomal templates showed that RNA polymerase II cannot traverse through nucleosomes [12]. On moderately active genes, H2A/H2B histones are exchanged at a much higher rate than H3/H4, suggesting that only H2A/H2B are displaced [13,14], whereas during intense transcription all core histones are displaced/exchanged at the transcribed regions [15]. Nucleosome dissociation could be induced either by direct contact of the polymerase molecule with a nucleosome core, or indirectly by the DNA topological stress generated during transcription [16]. The high concentration of chromatin in the nucleus and the well-known high affinity of excess histones for nucleosomes [17], had suggested in early studies the possibility that displaced H2A/H2B (and even H3/H4) could be transiently associated with the nucleosomes of chromatin regions located near the transcribed genes [18]. The spontaneous reactions of transfer of H2A/H2B and H3/H4 from nucleosomes containing excess histones to DNA [18], between partially dissociated nucleosomes [19], and to histone chaperones [20] could be involved in the mechanism of nucleosome reassembly after the passage of RNA polymerase.

Depletion of H2A/H2B dimers has been also suggested to occur during DNA replication and repair [21,22]. Time-resolved small angle X-ray scattering was used to determine transient structures of protein and DNA constituents during salt-induced disassembly of nucleosome core particles [23], which revealed asymmetric release of DNA from disrupted nucleosome cores, displaying different patterns of protein dissociation. Such kinetic intermediates have been suggested to be biologically important elements for gene regulation.

In pioneering classic assays it had been reported that the purified replication proteins of bacteriophage T4 allowed the *in vitro* replication of a nucleosome-containing DNA template without histone displacement [24], and that nucleosomes (or at least H3/H4 tetramers) of SV40 minichromosomes remained associated with DNA during the replication with eukaryotic enzymes [25]. On the other hand, from yeast *in vivo* studies it had been concluded that during chromatin replication the bulk of core histone octamers within old nucleosomes were dissociated [26]; the newly synthesized nucleosomes contained random mixtures of two H2A/H2B dimers (new or old) and one H3/H4 tetramer (new or old). More recently, it has been shown that the yeast histone H3 variant Cse4 undergoes *de novo* replacement in S phase [27].

Summarizing, despite the existence of a large amount of data reporting on the dynamic eviction of histones from DNA during replication and transcription [28], there is also compelling evidence that a complete dissociation of nucleosome cores might not always occur. However, even in these cases, it is reasonable to assume that the normal structure of the nucleosome must be strongly perturbed to allow the transient formation of single-stranded DNA (ssDNA). This implies that the histones remaining bound to DNA may interact with ssDNA. Moreover, a temporary interaction between ssDNA and the histones released from nucleosomes involved in replication or transcription cannot be excluded. Little is known about these possibilities because only a few early reports have been devoted to the study of the interaction of histones with ssDNA [29-32]. In this work we have used different techniques to carry out a detailed analysis of the association of core histones with the ssDNA of bacteriophage M13. We have also investigated the interaction of histones with the purified (+) and (–) strands of a cloned DNA fragment from nucleosomal origin.

2. Materials and methods

2.1. Materials

Except where otherwise indicated, reactions were performed at room temperature (20 °C) and reagents were purchased from Sigma-Aldrich Corporation (St. Louis, MO, USA).

2.2. Preparation of nucleosomes, histones, and M13 DNA

Core histones, H2A/H2B and H3/H4 pairs, oligonucleosomes and core particles were obtained from chicken erythrocyte nuclei as previously described [18,19]. The result of a typical core histone preparation is shown in Supplementary Fig. 1. Circular ssDNA and double-stranded DNA (dsDNA) from bacteriophage M13mp18 were isolated and

analyzed by conventional procedures [33]. The concentrations of DNA solutions were determined spectrophotometrically, using an A_{260} of 20 and 28 for 1 mg/ml solutions of dsDNA and ssDNA [34], respectively.

2.3. Linearization of ssM13mp18 and dsM13mp18 DNAs

Digestion with *EcoRI* (Roche Diagnostics GmbH, Mannheim, Germany), which has a single recognition site in M13mp18, was the strategy chosen to linearize the circular DNA forms. In this work M13 dsDNA has been used always in its linear form. To generate a double strand region around the *EcoRI* site in the ssDNA species, 100 µg of ssM13mp18 (6,407 bases) were mixed with 0.54 µg of the 20-base oligonucleotide 5'-CGAGCTCGAATTCGTAATCA-3' (approximate molar ratio 1:2), and left to hybridize at room temperature for 30 min prior to restriction enzyme digestion and analysis in agarose gels (Supplementary Fig. 2).

2.4. Purification of the (+) and (–) strands of the core NX1 DNA fragment

The NX1 DNA insert [35] was excised from the M13 vector by digestion with *EcoRI* and *BamHI* (Roche Diagnostics GmbH) and further amplified using the pBluescript SK(+) vector (Agilent, Santa Clara, CA, USA). Finally, *EcoRI* and *BamHI* were used to remove the insert from this plasmid. The linear plasmid was separated from the NX1 fragment by precipitation with 7.5% polyethylene glycol in TE buffer (1 mM EDTA, 10 mM Tris-HCl, pH 7.5) containing 0.55 M NaCl. The resulting NX1 DNA was phenol-extracted twice, precipitated with isopropanol, and washed with 70% ethanol. The (+) and (–) strands of NX1 DNA were purified by polyethylene glycol precipitation as described elsewhere [36].

2.5. Electrophoretic and turbidimetric analysis of DNA-histone complexes

Unless otherwise indicated in the corresponding figure legends, all titrations were performed in TE buffer supplemented with 0.15 M NaCl. In those experiments involving NX1 DNA the buffer contained 6.6% sucrose and BSA at the same concentration as histones. Histones were mixed with DNA and incubated at room temperature for 30 min before either measuring A_{320} (for turbidimetry analysis) or loading onto electrophoresis gels. NX1 DNA samples were analyzed in nondenaturing, 15 cm long 6% polyacrylamide-Tris/borate/EDTA (TBE) gels, as described previously [18]. Samples containing M13 DNA were electrophoresed in nondenaturing, 25 cm long 1.4% agarose-TBE gels, at 250 V for 3 h in an ice bath. The DNA was stained with ethidium bromide and the gel was photographed over an ultraviolet light. For quantitative analysis of relative DNA

amounts several exposures were obtained, selecting for scanning (Shimadzu CS-9000 densitometer) those photographic negatives where all DNA bands were below film saturation (Supplementary Fig. 3). The inverse of band intensity relative to t_0 was represented as % DNA-histone association.

2.6. Transmission electron microscopy (TEM)

M13 ssDNA or linearized M13 dsDNA was mixed at room temperature with core histones (histone to DNA weight ratio was 1.2 for dsDNA and 2.4 for ssDNA) in TE buffer containing 2 M NaCl, 0.2 mM EDTA, and 5 mM triethanolamine hydrochloride, pH 7.4. The NaCl concentration was progressively decreased by dilution: 1.6 M (30 min), 1.2 M (1 h), 0.85 M (1 h), 0.75 M (1 h), 0.6 M (1 h), 0.45 M (1 h), and 0.2 M (2 h). The final DNA concentrations were 24 µg/ml (dsDNA) and 21 µg/ml (ssDNA). Spread preparations of the resulting samples and oligonucleosomes were prepared as previously described [18]. All samples were fixed by treatment with 0.2% glutaraldehyde (Merck KGaA, Darmstadt, Germany) for about 15 h at 4 °C in the presence of 0.2 M NaCl, 0.2 mM EDTA, and 5 mM triethanolamine hydrochloride, pH 7.4. Fixed samples were diluted with the fixation buffer containing 10 mM NaCl to a final concentration of 2-0.8 µg DNA/ml. Carbon-coated 400-mesh copper grids made hydrophilic by a 5-min treatment with 0.002% Alcian blue 8GX (SERVA Electrophoresis GmbH, Heidelberg, Germany) and used within 30 min were placed on a Parafilm sheet and overlaid with a 10-µl drop of each sample. After 5 min of adsorption, excess liquid was removed with the edge of a filter paper and the grids were washed by immersion in water for 5 min, dehydrated in ethanol for 2-3 s, and allowed to dry on a filter paper. Finally, the grids were rotary-shadowed with platinum at an angle of about 6°. Micrographs were taken at a magnification of 30,000× with a Hitachi H7000 electron microscope operated at 75 kV.

2.7. Atomic force microscopy (AFM)

Highly oriented pyrolytic graphite (HOPG) substrates (ZYB-SS-2; TipsNano, Estonia) were coated with octadecylamine (ODA) by means of vapor deposition according to a method published elsewhere [37,38]. Briefly, ca. 5 µg ODA on a microscope slide was placed on a heater plate at a temperature of 100 °C. After melting of the ODA, freshly cleaved HOPG was placed 4 cm above the ODA droplet face down for 5-20 seconds while capped with a beaker. Prior to the application of DNA the modified substrates were analyzed by AFM in order to select those that exposed large (<100 × 100 nm^2) crystalline domains. For free DNA images, 10 µl of M13 ssDNA (0.5 ng/µl deionized water) was applied to the ODA-

functionalized HOPG substrates, which after 10 min incubation were gently dried with filter paper under N_2 flow. For histone-DNA samples, 0.9 ng/µl ssDNA was incubated with 2.6 ng histone/µl and allowed to react for 15 min. Finally, 10 µl of M13 ssDNA-histone solution was applied to the ODA-functionalized HOPG substrates, which after 10 min incubation were gently dried with filter paper under N_2 flow. All images were acquired in AFM tapping mode of operation under ambient conditions using a Multimode 8 AFM (Bruker, Santa Barbara, CA, USA) and Tap300Al Cantilevers (BudgetSensors, Sofia, Bulgaria).

2.8. Magnetic tweezers (MT) assays

A commercial MT instrument (Pico Twist, Lyon, France) was used with a custom-made flow cell that is briefly described below. A glass coverslip was first cleaned and covalently coated with Sigmacote in a desiccator to achieve a hydrophobic surface. With 70 µm thick, double-adhesive tape (Montex DX1; X-film, Lindlar, Germany) and a 100 µm thick polyester cover (3570; Zweckform, Oberlaindern, Germany) we then built a flow cell with 5 mm wide, 50 mm long and 70 µm thick chamber. Next, a 200 µg/ml anti-digoxigenin (anti-dig; Roche, Penzberg, Germany) solution was flushed into the flow cell and allowed to non-specifically adsorb onto the hydrophobic glass surface during incubation for at least 2 hours at 37 °C. Finally, the flow cell was rinsed with 10 mM PBS, pH 7.4, containing 137 mM NaCl and 2.7 mM KCl, and supplemented with 0.2% BSA, 0.1% Tween® 20, 5 mM EDTA and 10 mM NaN_3 in order to block and passivate further non-specific bonds during the experiments. The resulting flow cell was stored at 4 °C.

For MT experiments with dsDNA, λ DNA fragments (New England BioLabs, Frankfurt, Germany) were functionalized following existing protocols [39], at one end with several biotins (Biotin-14-dCTP; Meta-Bion GmbH, Steinkirchen, Germany) and at the other end with several digoxigenins (Dig-11-dUTP; Roche), and stored in 10 mM PBS buffer (+137 mM NaCl, +2.7 mM KCl, pH 7.4 at 25 °C) at 4 °C. This dsDNA was linked via anti-dig to the surface of the custom-made flow cell, and streptavidin-coated superparamagnetic beads (Dynabeads® MyOne™ Streptavidin C1, 1 µm diameter; Thermo Fisher, Waltham, USA) bound to the biotin-functionalized DNA end were used as magnetic handle. The beads (10 mg/ml) were gently mixed with 60 pM λ DNA in MT buffer (10 mM PBS containing 137 mM NaCl and 2.7 mM KCl, supplemented with 0.1 mg/ml BSA and 0.1% Tween® 20, pH 7.4 at 25 °C) and incubated for 15 min. Prior to every experiment the structural integrity of each probed DNA molecule (nick-free) and its torsionally constrained immobilization were verified, a reference hat-curve was acquired by MT overwinding experiments, and the DNA contour length was finally determined by means of stretching experiments.

For MT experiments with ssDNA, and following the removal of the two short oligonucleotide fragments resulting from *EcoRI* digestion (Supplementary Fig. 4A), M13 ssDNA was functionalized with a biotinylated oligonucleotide (5'-B-CTGTGTGAAAT-B-3'; B=biotin, C/T=dC/dT-biotin, Meta-Bion) at the 3' end and with two digoxigenin-labeled oligonucleotides (5'-D-AGCTCGAATT-D-3' and 5'-D-ATCCCCGGGT-D-3'; D=digoxigenin, Meta-Bion) at the 5' end (Supplementary Fig. 4B), and stored until use at 4 °C in 10 mM PBS, pH 7.4, containing 137 mM NaCl and 2.7 mM KCl.

For single-molecule experiments, M13 ssDNA was attached in a separate vial to 10 mg/ml streptavidin-coated 2.8 µm superparamagnetic microbeads (Dynabeads® M280; Thermo Fisher) via the specific biotin-streptavidin bond. When flushed into the flow cell, ssDNA-microbeads were allowed to bind the anti-dig coated surface through the specific digoxigenin-anti-dig interaction. Properly immobilized M13-microbead constructs were trapped in the magnetic field and stretched for functional control. These force-extension (F-d) experiments were performed from 0.3 pN up to about 30 pN, whereas F-d control assays with λ dsDNA were performed from 10^{-3} pN to 10 pN. To estimate the DNA contour and persistence lengths, the experimental data were fitted to the (extended) worm-like chain model [40-42].

WLC: $$\frac{FL_P}{k_BT} = \frac{1}{4}\left[\left(1-\frac{d}{L_0}\right)^{-2} - 1\right] + \frac{d}{L_0} \qquad (1)$$

extended WLC: $$d = L_0\left[1 - \frac{1}{2}\left(\frac{k_BT}{FL_P}\right)^{1/2} + \frac{F}{K_0}\right] \qquad (2)$$

Here, F denotes the force, k_BT the thermal energy, d the DNA end-to-end distance, K_0 the stretching modulus, and L_P and L_0 are the persistence and contour length, respectively. Preset forces were 0.4 pN and 15 pN for overwinding and extension-time experiments, respectively. A 10 µM core histones plus linker H1 histone solution was diluted to the applied concentrations with MT buffer, flushed into the chamber and incubated for 15 min to achieve thermodynamic equilibrium. All experiments were performed in MT buffer.

2.9. Micrococcal nuclease digestion

M13 dsDNA or ssDNA at a concentration of 68 µg/ml was digested with micrococcal nuclease (3.6 or 0.5 UW/µg dsDNA or ssDNA, respectively) in the absence or in the presence of core particle histones at a w/w ratio histone:DNA of 1:1 or 2:1 for dsDNA and

ssDNA, respectively. The samples were incubated for 5 h in TE buffer containing 0.2 M NaCl and 10 mM $CaCl_2$ before adding micrococcal nuclease and incubating for the times indicated (1, 11, 20, and 45 min). To stop the reaction, nuclease-treated samples were digested with proteinase K in the presence of 0.2% SDS, and the DNA EtOH-precipitated and resuspended in 50 µl of deionized formamide. After heating for 2 min at 100 °C the resulting DNA was analyzed in a 7% polyacrylamide/formamide denaturing gel stained with ethidium bromide as described elsewhere [43].

3. Results

3.1. Binding of core histones to high molecular mass ssDNA

The binding of core particle histones to M13 ssDNA and dsDNA was initially monitored by measuring in agarose gels the decrease in intensity of the corresponding free DNA bands with the addition of increasing histone amounts (Fig. 1A). Closed and linear DNA forms were observed to complex histones with similar avidity; the closed ssDNA form was generally used for gel densitometric analysis because of its larger amount in our preparations and its distinct electrophoretic mobility relative to linear dsDNA. These titration studies invariably exhibited the expected sigmoidal profiles characteristic of a cooperative binding between histones and DNA (Fig. 1B), where at higher concentrations the equilibrium was more displaced towards the formation of nucleoproteic complexes. Preliminary analysis of the data indicated that, considering identical DNA masses, ssDNA required twice as much histone than dsDNA for equal association dynamics. Applying this transformation to the data from four independent assays done at different DNA concentrations confirmed that for a given *x* DNA mass, dsDNA and ssDNA have similar affinity for core histones when these are present with *y:x* and *2y:x* masses, respectively (Fig. 1C). DNA aggregation turbidimetric analyses confirmed this observation, and when the data obtained were represented considering the molar concentration of histone octamers (assuming that the four core histones associate with DNA in the equimolar ratio found in native nucleosomes) *vs* nucleotides or base pairs for ssDNA and dsDNA respectively, the titration curves were coincident (Fig. 2A). The length of M13 ssDNA varies as a function of the buffer salt concentration [44]. However, according to TEM images, under our ionic strength conditions similar lengths are observed for the same number of bases or base pairs in ssDNA and dsDNA polymers, respectively (Supplementary Fig. 5). Taken together, the above results suggested that the length of DNA (expressed in number of ssDNA nucleotides and dsDNA base pairs) associated with a particular histone mass is the same for both ssDNA and dsDNA.

The observed binding cooperativity permitted the calculation of thermodynamic parameters such as the nucleation constant *K* [45], and the cooperativity factor *ω*, which expresses the relative affinity of a ligand for a contiguous binding site. Thus, when the next binding site is already occupied the binding constant *K'* becomes the association constant Kω. In the case of a cooperative binding the product *Kω* is related with the ligand concentration at the titration midpoint, $L_{T,½}$, according to the following equation:

$$\frac{1}{K\omega} = L_{T,1/2} - \left(\frac{N}{2n}\right) \qquad (3)$$

where *n* is the binding site size (168 nucleotides or base pairs per histone octamer [46]) and *N* its concentration. Application of the equation [3] to the titration curves from Fig. 2A provided similar *Kω* values for dsDNA and ssDNA (2.5×10^7 and 2.1×10^7 M^{-1}, respectively). The separate values for *K* and *ω* can be obtained by fitting the experimental data to the following theoretical equation [4] for the quantitative analysis of the cooperative binding of proteins to nucleic acids (Fig. 2B) [47]:

$$\frac{v}{L} = K(1-nv)\left[\frac{(2\omega-1)(1-nv)+v-R}{2(\omega-1)(1-nv)}\right]^{n-1}\left[\frac{1-(n+1)v+R}{2(1-nv)}\right]^{2} \qquad (4)$$

where $R = [[1 - (n + 1)v]^2 + 4\omega v(1 - nv)]^{½}$, *v* is the binding density of the ligand (in moles of histone octamer per mole of nucleotide residue or base pair), and *L* is the free octamer concentration (in mol/l). The resulting values for *K* and *ω* are 5×10^3 M^{-1} and 5×10^3 for dsDNA and 3×10^3 M^{-1} and 7×10^3 for ssDNA, respectively.

To explore whether the interaction of histones with ssDNA is the result of molecular adsorption or of a nucleosome-like association, we characterized the resulting structures by electron microscopy and nuclease protection assays. Transmission electron microscope images of histone-ssDNA samples showed the presence of nucleosome-like particles that were similar to those observed in histone-dsDNA or native chromatin samples (Fig. 3). Micrococcal nuclease digestion studies indicated that in the presence of histones there was a significant protection of M13 ssDNA in front of the DNase (Fig. 4).

3.2. Atomic force microscopy of ssDNA and ssDNA-histone complexes

Because TEM images and DNase protection assays suggested the presence of nucleosome-like structures in ssDNA-histone samples, single-molecule AFM and MT assays were performed to further investigate this interaction. The structure and integrity of the M13 ssDNA

to be used in MT assays were first analyzed by AFM imaging, following a protocol whereby the DNA was immobilized on ODA-modified HOPG and imaged under ambient conditions [37,38]. Typical AFM topography images showed highly ordered domains of parallel oriented ODA on HOPG that interacted via their positively charged amine groups with the negatively charged M13 ssDNA backbone, resulting in stretched and axially oriented ssDNA molecules (Fig. 5A). Without the counterionic ODA surfactant layer the ssDNA exhibited a featureless random coil-like structure due to self-hybridization effects (data not shown). In contrast, AFM images of preassembled histone-M13 ssDNA complexes immobilized on ODA-modified HOPG did not show individual and stretched ssDNA molecules, revealing instead the presence of globular structures 5 ± 1 nm in height (Fig. 5B and C), similar to those observed in TEM images of histone-ssDNA samples and consistent with the disc-shaped dimensions of nucleosomes (11 × 5.7 nm, [48]).

3.3. Magnetic tweezers analysis of ssDNA-histone interaction

MT assays were done to explore histone-DNA interactions in more detail. In histone-free control and reference experiments, stretching and overwinding curves of double-stranded λ DNA resulted in polymer elasticity and torsional curves as expected for linear, nick-free dsDNA (Fig. 6A and B), with a persistence length of L_P = 48 nm and the plectonemic overwinding of the molecule associated with a shortening of the molecular end-to-end distance ("hat curve"). In contrast, MT experiments with single-stranded M13 DNA exhibited considerably softer elastic properties with a persistence length of only L_P = 7 nm in molecular stretching experiments (Fig. 6C). In addition, torsional overwinding experiments with ssDNA led to a rotation-independent constant end-to-end distance since the DNA polymer can rotate around its sugar backbone in idle state (Fig. 6D).

The addition of 5 nM histone to a single dsDNA molecule held in the MT trap at a preset force of 0.5 pN resulted in a shortening of the dsDNA along time with distinct ca. 100-nm steps (Fig. 7A and Supplementary Fig. 6). This step size can be rationalized by the fact that in the nucleosome 147 bp of dsDNA (×0.34 nm/bp ≈ 50 nm) wrap around the core particle [3], and therefore a 100 nm step would correspond to the formation of a distinct nucleosome pair. The formation of a nucleosome pair can be topologically explained since the wrapping of a torsionally constrained dsDNA molecule (as we have in the MT) around a histone core induces torsional twists that can be released by the formation of two counter-rotating nucleosome wrappings. A similar experiment with ssDNA could not be conducted since ssDNA undergoes self-hybridization under such low external forces, leading to shortening of the molecular end-to-end distance in the absence of histones.

In contrast, ssDNA was found to be amenable to analysis in single-molecule stretching experiments performed under higher forces of up to 20 pN (Fig. 7B and C). In the presence of 10 nM histones, MT stretching assays clearly indicated a significantly shorter end-to-end ssDNA length (Fig. 7B), suggesting interaction of histones with ssDNA accompanied by the formation of three-dimensional nucleoprotein structures. In a different MT assay, where the ssDNA fragments were kept at a constant preset force of 15 pN over time (Fig. 7C), bare M13 ssDNA exhibited discrete end-to-end distance jumps that can be attributed to partial disentangling of ssDNA secondary structure. In contrast, ssDNA-histone complexes containing 10 nM protein that were kept at a constant force of 15 pN, exhibited a stable and constant end-to-end DNA distance. The presence of 500 nM histone led to a fully compacted ssDNA with negligible contour length that could not be disentangled (data not shown). These results support the hypothesis that ssDNA and histones form some type of organized nucleosome-like structure.

3.4. Competitive association of ssDNA and dsDNA with core histones

Competition experiments were done where increasing core histone amounts were added to a solution containing equal masses of ssDNA and dsDNA (52 µg/ml of each species, i.e. a molar ratio ssDNA bases:dsDNA base pairs 2:1), and the electrophoretic mobility of the resulting DNA/histone complexes was analyzed in non-denaturing agarose gels (Fig. 8A). In agreement with the association results obtained separately with each DNA form for this high concentration (Fig. 1B), at a histone:ssDNA w/w ratio of 0.75 (the same ratio as for histone:dsDNA because there are equal amounts of both species) all the dsDNA was complexed with histones whereas the ssDNA was not associated to histones as indicated by their respective electrophoretic mobilities. At a histone:ssDNA ratio of 2.25 (w/w) all the ssDNA was associated to histones; when subtracting the 0.75 histone equivalents bound to dsDNA, the remaining 1.5 equivalents are consistent with the histone amount required to complex the twice as high molar amount of ssDNA relative to dsDNA present in the solution. When both DNA species were together in the same solution in equimolar amounts (i.e. same number of bases and base pairs, or twice the mass of dsDNA relative to ssDNA), it could be observed that upon addition of increasing amounts of core histones, these complexed both ssDNA and dsDNA with apparently equal affinities (Fig. 8B and C). The cooperative binding of histones to DNA resulted in relative large inter-experiment variability of the data obtained (Fig. 8C), probably reflecting small concentration differences in the histone solution which was freshly prepared before each assay. Because of the need to load all samples into the gels after similar aggregation times (30 min), preference was given to running together ssDNA/dsDNA pairs instead of two replicas of the same DNA species in

order to minimize the error for the interaction under study (i.e. the comparative affinity of histones for ssDNA *vs* dsDNA). The addition of large amounts of ssDNA to aggregated dsDNA-core histone complexes induced the complete release of the dsDNA previously associated with histones (Fig. 9A). In contrast, dsDNA could not dissociate core histones from ssDNA (Fig. 9B). Taking into account that the apparent association constant is essentially the same for both ssDNA- and dsDNA-histone complexes, these observations suggest that ssDNA:histone complexes are more stable in front of free dsDNA than dsDNA:histone complexes are in front of free ssDNA.

3.5. Binding of core histones to the purified (+) and (–) strands of a cloned nucleosome core DNA

To characterize more in detail the type of structure formed by histones on ssDNA we performed titration studies in non-denaturing 6% polyacrylamide gels using the cloned 158-bp NX1 DNA sequence that was forming a nucleosome *in vivo* [36] (Fig. 10). dsNX1 was complexed with a similar kinetics by core particle histones (Fig. 10A) and by the pairs H3/H4 (Fig. 10B) and H2A/H2B (Fig. 10C); however, the corresponding nucleoproteic complexes formed exhibited different electrophoretic patterns, suggesting the formation of different structures with each histone composition. Nucleosome and nucleosome-like bands were observed at about half the electrophoretic mobility than naked nucleosomal dsDNA. The two strands of the NX1 fragment were purified by polyethylene glycol differential precipitation [36], through a protocol involving treatment of the (–) strand with HCl (pH 1.8). Since it had been described that DNA can be partially depurinated with acid and then cleaved at depurination sites with 0.5 M NaOH [49], we examined whether the purified (–) strand used in this study was depurinated. The (–) strand was incubated at room temperature for 15 min with 0.5 M NaOH in the presence of 1 M NaCl [49] and the resulting sample was analyzed in a polyacrylamide gel. The intensity of the band corresponding to the (–) strand was unchanged by the alkaline treatment (not shown), indicating that the extent of depurination was negligible. As expected, the (–) and (+) strands used in this study reassociated rapidly to form the typical band corresponding to NX1 dsDNA (Fig. 10D).

The association of core histones with NX1 dsDNA in the presence of 0.2 M NaCl produced a decrease in the intensity of the free DNA band, a well-defined nucleosome band, and aggregated material that did not enter the gel (Fig. 10A). Under the same ionic strength conditions, increasing amounts of core histones caused a progressive decrease in the intensity of the band corresponding to the (+) strand of the NX1 fragment (Fig. 10D). These titration results obtained for the (+) strand were consistent

with the data obtained with M13 DNA, according to which an amount (w/w) of core particle histones double than that needed for dsDNA was required in order to complex ssDNA. As previously reported [35] the (+) strand had a significantly greater affinity for histones than the (–) strand (Fig. 10D), probably as a result of their different sequences. NX1 ssDNA-histone titrations did not reveal the appearance of nucleosome-like bands. This is likely due to neutralization of the negative charges of the 158-base NX1 ssDNA fragment, which are almost completely cancelled by the 148 positive charges of a histone octamer [50], resulting in a species with virtually no electrophoretic mobility. Similar results were obtained for the H2A/H2B and H3/H4 pairs (Fig. 10E).

4. Discussion

The binding assays reported here demonstrate that histones have high affinity for ssDNA at physiological ionic strength. These studies, together with competitive association results, indicate that the binding constant is roughly the same for both M13 dsDNA and M13 ssDNA, strongly suggesting that in the cell nucleus histones may interact with ssDNA. The association constant determined for histone-ssDNA affinity does not differ significantly from those obtained for other molecules binding dsDNA [51,52] and ssDNA [53]. Although our results indicate that ssDNA-histone complexes have a high tendency to aggregate under physiological salt concentrations, at lower ionic strength structures resembling nucleosome core particles are observed by electron microscopy, and the interaction with histones protects ssDNA from micrococcal nuclease digestion. Since the present knowledge on the replication and transcription of chromatin suggests that interaction of histones with ssDNA can take place only transiently and in some cases only before the partial or complete removal of histones induced by these processes, *a priori* it seems unlikely that histones can interact *in vivo* with ssDNA stretches long enough to produce complete nucleosomal structures. However, structural studies of other authors have shown that the binding of core histones to ssDNA can produce nucleosome-like complexes [29-32], in agreement with the conclusions that can be obtained from the data presented here. Optical/magnetic tweezers have been used to study the force-induced dynamic response of canonical nucleosomes to different mechanical constraints [54-56], but this powerful technique had not been applied so far to the study of histone-ssDNA interactions. The pioneering magnetic tweezers results presented here support the hypothesis that histones do not merely adsorb on ssDNA, but they induce instead the formation of some type of structure leading to shortening of the DNA and stabilization of its secondary structure; both observations are consistent with the existence in histone-ssDNA complexes of a nucleosome-like entity (Fig. 11A).

The observation that equal lengths of ssDNA and dsDNA complex equal histone masses suggests that histones can be bound to either one of these DNA forms without extensive modification of their structure. This could be related to the sequential arrangement of histones along DNA in the nucleosome core particle inferred from DNA-histone crosslinking experiments and from the structural analysis of core particle and histone octamer crystals [57]. It has been reported that this histone organization is maintained even when the nucleosome structure is perturbed with denaturing agents [58] and when nucleosomes are located within transcriptionally active heat-shock *Drosophila* genes [59]. Repositioning of histone octamers during transcription has been described to occur along the same DNA segment by sliding [60], a process only considered so far for dsDNA but which can also unfold on ssDNA regions of transcribed genes. The association of histones with a constant length of either dsDNA or ssDNA may facilitate transcription without alteration of the linear order of histones along DNA (Fig. 11B). Results obtained in titration and competitive association experiments under the ionic strength conditions of transcription indicate that RNA has a high affinity for core histones and therefore can compete for histones in the presence of DNA [35]. However, under the same transcription conditions and with a weight ratio of the synthesized RNA to the DNA template of around 7:1, the synthesized RNA did not associate with histones [35]. Here we have observed significant histone transfer from dsDNA to ssDNA at a ssDNA:dsDNA weight ratio below 1:1, suggesting that although RNA might interact transiently with histones, these could have a much stronger preference for ssDNA.

In contrast to the well-established fact that the dsDNA sequences in a genome are a determinant of nucleosome organization and positioning [60,61], to the best of our knowledge there are no studies on the possible differential affinity of ssDNA sequences for histones. However, we have found that for a short DNA of 148 base pairs like the NX1 fragment each of the two complementary strands has different affinities for histones. Nevertheless, it is to be expected that over long DNA stretches, such as those in M13, high and low affinities for histones will be randomly distributed throughout the sequences of both strands, cancelling each other and providing an overall ssDNA-histone interaction that is not dependent on sequence. Although the observed binding energy difference between the (+) and (–) strands of the nucleosome DNA fragment used in this study is relatively small (ca. 1 kcal/mol) [35], it is high enough to produce a preferential association of histones with one of the strands. Comparable energy differences allow the preferential binding of histones to dsDNA containing nucleosome positioning sequences in competitive reconstitution experiments [62]. From a kinetic point of view, low energy differences may be useful for functional processes involving nucleosomes. Our observations are compatible with crosslinking results indicating that core

histones in the nucleosome are bound within discrete DNA segments mainly to one DNA strand, but can occasionally jump to bind the complementary strand [63], and suggest that the association of histones with ssDNA could occur spontaneously during replication and transcription of chromatin.

Acknowledgements

We thank the staffs of the Servei de Seqüenciació de DNA (Centre d'Investigació i Desenvolupament, CSIC) and of the Servei de Microscòpia Electrònica (Universitat Autònoma de Barcelona) for their assistance. We acknowledge technical support from Helene Schellenberg, Christoph Pelargus and Niklas Biere. We are indebted to Prof. Joan-Ramon Daban for valuable discussions regarding the biophysical characterization of the interaction of histones with ssDNA and to Dr. Salvador Bartolomé for his help with the densitometries of gel electrophoresis bands. IBEC and ISGlobal are members of the CERCA Programme, Generalitat de Catalunya.

Funding

This work was supported in part by grants BIO2002-00128 from the Ministerio de Economía y Competitividad, Spain, which included Fondo Europeo de Desarrollo Regional funds, and 2009SGR-760 from the Generalitat de Catalunya, Spain.

References

[1] Ö. Deniz, O. Flores, M. Aldea, M. Soler-López, and M. Orozco, Nucleosome architecture throughout the cell cycle, Sci. Rep., 6 (2016) 19729.

[2] O.I. Kulaeva, F.K. Hsieh, H.W. Chang, D.S. Luse, and V.M. Studitsky, Mechanism of transcription through a nucleosome by RNA polymerase II, Biochim. Biophys. Acta, 1829 (2013) 76-83.

[3] P. Zhu and G. Li, Structural insights of nucleosome and the 30-nm chromatin fiber, Curr. Opin. Struct. Biol., 36 (2016) 106-115.

[4] J. Zlatanova, T.C. Bishop, J.M. Victor, V. Jackson, and K. van Holde, The nucleosome family: dynamic and growing, Structure, 17 (2009) 160-171.

[5] A.J. Bannister and T. Kouzarides, Regulation of chromatin by histone modifications, Cell Res., 21 (2011) 381-395.

[6] A.P. Wolffe and J.J. Hayes, Chromatin disruption and modification, Nucleic Acids Res., 27 (1999) 711-720.

[7] T.W. Flanagan and D.T. Brown, Molecular dynamics of histone H1, Biochim. Biophys. Acta, 1859 (2016) 468-475.

[8] A. Wunsch and V. Jackson, Histone release during transcription: acetylation stabilizes the interaction of the H2A–H2B dimer with the H3–H4 tetramer in nucleosomes that are on highly positively coiled DNA, Biochemistry, 44 (2005) 16351-16364.

[9] A. Sivolob and A. Prunell, Nucleosome conformational flexibility and implications for chromatin dynamics, Philos. Trans. R. Soc. Lond. A Math. Phys. Eng. Sci., 362 (2004) 1519-1547.

[10] G.M. Nam and G. Arya, Free-energy landscape of mono- and dinucleosomes: enhanced rotational flexibility of interconnected nucleosomes, Phys. Rev. E, 93 (2016) 032406.

[11] X. Liu, D.A. Bushnell, D. Wang, G. Calero, and R.D. Kornberg, Structure of an RNA polymerase II–TFIIB complex and the transcription initiation mechanism, Science, 327 (2010) 206-209.

[12] C.H. Chang and D.S. Luse, The H3/H4 tetramer blocks transcript elongation by RNA polymerase II *in vitro*, J. Biol. Chem., 272 (1997) 23427-23434.

[13] O.I. Kulaeva, D.A. Gaykalova, and V.M. Studitsky, Transcription through chromatin by RNA polymerase II: histone displacement and exchange, Mutat. Res., 618 (2007) 116-129.

[14] H. Kimura and P.R. Cook, Kinetics of core histones in living human cells: little exchange of H3 and H4 and some rapid exchange of H2B, J. Cell Biol., 153 (2001) 1341-1354.

[15] Y. Katan-Khaykovich and K. Struhl, Splitting of H3–H4 tetramers at transcriptionally active genes undergoing dynamic histone exchange, Proc. Natl. Acad. Sci. U. S. A., 108 (2011) 1296-1301.

[16] D.J. Clark and B.P. Leblanc, Analysis of DNA supercoiling induced by DNA–protein interactions, in: B.P. Leblanc and S. Rodrigue (Eds.), DNA-Protein Interactions: Principles and Protocols, Springer, New York, NY, 2015, pp. 161-172.

[17] H. Eisenberg and G. Felsenfeld, Hydrodynamic studies of the interaction between nucleosome core particles and core histones, J. Mol. Biol., 150 (1981) 537-552.

[18] A.M. Aragay, X. Fernàndez-Busquets, and J.R. Daban, Different mechanism for *in vitro* formation of nucleosome core particles, Biochemistry, 30 (1991) 5022-5032.

[19] A.M. Aragay, P. Diaz, and J.R. Daban, Association of nucleosome core particle DNA with different histone oligomers, J. Mol. Biol., 204 (1988) 141-154.

[20] Z.A. Gurard-Levin, J.P. Quivy, and G. Almouzni, Histone chaperones: assisting histone traffic and nucleosome dynamics, Ann. Rev. Biochem., 83 (2014) 487-517.

[21] D.M. MacAlpine and G. Almouzni, Chromatin and DNA replication, Cold Spring Harb. Perspect. Biol., 5 (2013) a010207.

[22] Y. Arimura, H. Tachiwana, T. Oda, M. Sato, and H. Kurumizaka, Structural analysis of the hexasome, lacking one histone H2A/H2B dimer from the conventional nucleosome, Biochemistry, 51 (2012) 3302-3309.

[23] Y. Chen, J.M. Tokuda, T. Topping, J.L. Sutton, S.P. Meisburger, S.A. Pabit, L.M. Gloss, and L. Pollack, Revealing transient structures of nucleosomes as DNA unwinds, Nucleic Acids Res., 42 (2014) 8767-8776.

[24] C. Bonne-Andrea, M.L. Wong, and B.M. Alberts, *In vitro* replication through nucleosomes without histone displacement, Nature, 343 (1990) 719-726.

[25] T. Krude and R. Knippers, Transfer of nucleosomes from parental to replicated chromatin, Mol. Cell. Biol., 11 (1991) 6257-6267.

[26] V. Jackson, *In vivo* studies on the dynamics of histone-DNA interaction: evidence for nucleosome dissolution during replication and transcription and a low level of dissolution independent of both, Biochemistry, 29 (1990) 719-731.

[27] J. Wisniewski, B. Hajj, J. Chen, G. Mizuguchi, H. Xiao, D. Wei, M. Dahan, and C. Wu, Imaging the fate of histone Cse4 reveals de novo replacement in S phase and subsequent stable residence at centromeres, eLife, 3 (2014) e02203.

[28] C. Das and J.K. Tyler, Histone exchange and histone modifications during transcription and aging, Biochim. Biophys. Acta, 1819 (2013) 332-342.

[29] K.B. Palter and B.M. Alberts, The use of DNA-cellulose for analyzing histone-DNA interactions. Discovery of nucleosome-like histone binding to single-stranded DNA, J. Biol. Chem., 254 (1979) 11160-11169.

[30] K.B. Palter, V.E. Foe, and B.M. Alberts, Evidence for the formation of nucleosome-like histone complexes on single-stranded DNA, Cell, 18 (1979) 451-467.

[31] E. Caffarelli, P. De Santis, L. Leoni, M. Savino, and E. Trotta, Interactions of the histone octamer with single-stranded DNA. Sedimentation analysis and low-angle X-ray diffraction, Biochim. Biophys. Acta, 739 (1983) 235-243.

[32] E. Caffarelli, L. Leoni, and M. Savino, Folding of single-stranded DNA on the histone octamer, FEBS Lett., 181 (1985) 69-73.

[33] J.F. Sambrook and D.W. Russell, Molecular Cloning: A Laboratory Manual, Cold Spring Harbor Laboratory Press, Cold Spring Harbor, New York, 2001.

[34] S.L. Brenner, R.S. Mitchell, S.W. Morrical, S.K. Neuendorf, B.C. Schutte, and M.M. Cox, recA protein-promoted ATP hydrolysis occurs throughout recA nucleoprotein filaments, J. Biol. Chem., 262 (1987) 4011-4016.

[35] F. Gallego, X. Fernàndez-Busquets, and J.R. Daban, Mechanism of nucleosome dissociation produced by transcription elongation in a short chromatin template, Biochemistry, 34 (1995) 6711-6719.

[36] X. Fernàndez-Busquets and J.R. Daban, Purification of the two strands of a DNA fragment by polyethylene glycol precipitation, Biotechniques, 13 (1992) 686-688.

[37] E.V. Dubrovin, S. Speller, and I.V. Yaminsky, Statistical analysis of molecular nanotemplate driven DNA adsorption on graphite, Langmuir, 30 (2014) 15423-15432.

[38] E.V. Dubrovin, J.W. Gerritsen, J. Zivkovic, I.V. Yaminsky, and S. Speller, The effect of underlying octadecylamine monolayer on the DNA conformation on the graphite surface, Colloids Surf. B Biointerfaces, 76 (2010) 63-69.

[39] Y. Wang, A. Sischka, V. Walhorn, K. Tönsing, and D. Anselmetti, Nanomechanics of fluorescent DNA dyes on DNA investigated by magnetic tweezers, Biophys. J., 111 (2016) 1604-1611.

[40] S.B. Smith, L. Finzi, and C. Bustamante, Direct mechanical measurements of the elasticity of single DNA molecules by using magnetic beads, Science, 258 (1992) 1122.

[41] C. Bustamante, S.B. Smith, J. Liphardt, and D. Smith, Single-molecule studies of DNA mechanics, Curr. Opin. Struct. Biol., 10 (2000) 279-285.

[42] C. Bouchiat and M. Mézard, Elastic rod model of a supercoiled DNA molecule, Eur. Phys. J. E, 2 (2000) 377-402.

[43] T. Maniatis and A. Efstratiadis, Fractionation of low molecular weight DNA or RNA in polyacrylamide gels containing 98% formamide or 7 M urea, Methods Enzymol., 65 (1980) 299-305.

[44] A. Schaper, C. Urbanke, and G. Maass, Salt dependent changes in structure and dynamics of circular single stranded DNA of filamentous phages of *Escherichia coli*, J. Biomol. Struct. Dyn., 8 (1991) 1211-1232.

[45] G. Schwarz and F. Watanabe, Thermodynamics and kinetics of co-operative protein-nucleic acid binding, J. Mol. Biol., 163 (1983) 467-484.

[46] K.E. Van Holde, J.R. Allen, K. Tatchell, W.O. Weischet, and D. Lohr, DNA-histone interactions in nucleosomes, Biophys. J., 32 (1980) 271-282.

[47] J.D. McGhee and P.H. von Hippel, Theoretical aspects of DNA-protein interactions: co-operative and non-co-operative binding of large ligands to a one-dimensional homogeneous lattice, J. Mol. Biol., 86 (1974) 469-489.

[48] J.T. Finch, L.C. Lutter, D. Rhodes, R.S. Brown, B. Rushton, M. Levitt, and A. Klug, Structure of nucleosome core particles of chromatin, Nature, 269 (1977) 29-36.

[49] G.M. Wahl, M. Stern, and G.R. Stark, Efficient transfer of large DNA fragments from agarose gels to diazobenzyloxymethyl-paper and rapid hybridization by using dextran sulfate, Proc. Natl. Acad. Sci. U. S. A., 76 (1979) 3683-3687.

[50] A.D. Mirzabekov and A. Rich, Asymmetric lateral distribution of unshielded phosphate groups in nucleosomal DNA and its role in DNA bending, Proc. Natl. Acad. Sci. U. S. A., 76 (1979) 1118-1121.

[51] E.C. Cesconetto, F.S.A. Junior, F.A.P. Crisafuli, O.N. Mesquita, E.B. Ramos, and M.S. Rocha, DNA interaction with Actinomycin D: mechanical measurements reveal the details of the binding data, Phys. Chem. Chem. Phys., 15 (2013) 11070-11077.

[52] Y. Duan, Z. Gao, L. Wang, H. Wang, H. Zhang, and H. Li, Selection and identification of chloramphenicol-specific DNA aptamers by mag-SELEX, Appl. Biochem. Biotechnol., (2016) 1-13.

[53] S. Uchiyama, K. Kawahara, Y. Hosokawa, S. Fukakusa, H. Oki, S. Nakamura, Y. Kojima, M. Noda, R. Takino, Y. Miyahara, T. Maruno, Y. Kobayashi, T. Ohkubo, and K. Fukui, Structural basis for dimer formation of human condensin structural maintenance of chromosome proteins and its implications for single-stranded DNA recognition, J. Biol. Chem., 290 (2015) 29461-29477.

[54] S. Mihardja, A.J. Spakowitz, Y. Zhang, and C. Bustamante, Effect of force on mononucleosomal dynamics, Proc. Natl. Acad. Sci. U. S. A., 103 (2006) 15871-15876.

[55] P. Recouvreux, C. Lavelle, M. Barbi, N. Conde e Silva, E. Le Cam, J.M. Victor, and J.L. Viovy, Linker histones incorporation maintains chromatin fiber plasticity, Biophys. J., 100 (2011) 2726-2735.

[56] A. Bancaud, N. Conde e Silva, M. Barbi, G. Wagner, J.F. Allemand, J. Mozziconacci, C. Lavelle, V. Croquette, J.M. Victor, A. Prunell, and J.L. Viovy, Structural plasticity of single chromatin fibers revealed by torsional manipulation, Nat. Struct. Mol. Biol., 13 (2006) 444-450.

[57] K. Luger, A.W. Mäder, R.K. Richmond, D.F. Sargent, and T.J. Richmond, Crystal structure of the nucleosome core particle at 2.8 Å resolution, Nature, 389 (1997) 251-260.

[58] V.W. Zayetz, S.G. Bavykin, V.L. Karpov, and A.D. Mirzabekov, Stability of the primary organization of nucleosome core particles upon some conformational transitions, Nucleic Acids Res., 9 (1981) 1053-1068.

[59] V.M. Studitsky, A.V. Belyavsky, A.F. Melnikova, and A.D. Mirzabekov, The structure of nucleosomal core particles within transcribed and repressed gene regions, Nucleic Acids Res., 16 (1988) 11187-11205.

[60] J. Gutiérrez, R. Paredes, F. Cruzat, D.A. Hill, A.J. van Wijnen, J.B. Lian, G.S. Stein, J.L. Stein, A.N. Imbalzano, and M. Montecino, Chromatin remodeling by SWI/SNF results in nucleosome mobilization to preferential positions in the rat osteocalcin gene promoter, J. Biol. Chem., 282 (2007) 9445-9457.

[61] P.G. Yazdi, B.A. Pedersen, J.F. Taylor, O.S. Khattab, Y.H. Chen, Y. Chen, S.E. Jacobsen, and P.H. Wang, Nucleosome organization in human embryonic stem cells, PLoS ONE, 10 (2015) e0136314.

[62] F. Battistini, C.A. Hunter, I.K. Moore, and J. Widom, Structure-based identification of new high-affinity nucleosome binding sequences, J. Mol. Biol., 420 (2012) 8-16.

[63] V.V. Shick, A.V. Belyavsky, S.G. Bavykin, and A.D. Mirzabekov, Primary organization of the nucleosome core particles sequential arrangement of histones along DNA, J. Mol. Biol., 139 (1980) 491-517.

FIGURE LEGENDS

Fig. 1. Agarose gel studies of the association of core particle histones with M13 ssDNA and dsDNA. (**A**) Identical masses of M13 ssDNA and dsDNA were titrated with increasing amounts of core particle histones in TE buffer supplemented with 0.15 M NaCl. (**B**) In similar assays performed at different DNA concentrations, the resulting ethidium bromide-stained bands were densitometered and the inverse of band intensity relative to t_0 was represented as % DNA-histone association. To simplify the graph, only the ssDNA data are shown for the two lowest DNA concentrations; the corresponding curves obtained with equal respective dsDNA masses were displaced as observed for the highest concentration of 44 µg/ml (i.e. dsDNA required for complexation half the histone mass than an equal amount of ssDNA). (**C**) Linear regression representation of the titration with core histones of M13 ssDNA and dsDNA at four different concentrations. Each data point corresponds to identical ssDNA and dsDNA masses incubated with a histone mass that was always double in the ssDNA sample relative to the dsDNA sample. In each of the four individual experiments the data represented correspond to the region of cooperative binding, which runs from the data point before association to histones was first detected in any DNA species to the data point where one of the two DNAs reached 100% complexation.

Fig. 2. Turbidimetric studies of the association of core particle histones with M13 ssDNA and dsDNA. (**A**) The represented histone:DNA ratio corresponds to core histone octamers (1.09×10^5 Da/octamer) *vs* base pairs (6.50×10^2 Da/bp) or nucleotides (3.25×10^2 Da/b) for dsDNA and ssDNA respectively. (**B**) Fitting of the titration curves from panel **A** according to McGhee and Von Hippel [47]. Theoretical values are represented by solid circles and experimentally obtained values by empty symbols.

Fig. 3. Transmission electron microscopy of the structures formed between core particle histones and M13 ssDNA. Native chicken erythrocyte oligonucleosomes (chromatin) and histone + M13 dsDNA samples are included as controls. We show in the bottom panels two images of ssDNA + histone samples, one with the most abundantly seen isolated globular structures and a second one with an uncommon example of a string of globular shapes on ssDNA resembling nucleosomes in chromatin (arrowhead).

Fig. 4. Electrophoretic analysis of micrococcal nuclease digestion of M13 ssDNA and dsDNA complexed with core particle histones ((+) histones). Digestion of the same samples in the absence of histones is shown as a control ((–) histones).

Fig. 5. Typical AFM topography images taken on ODA-modified graphite. (**A**) Linearized M13 ssDNA that aligns with the striped ODA domain structure on graphite is shown to check the integrity of ssDNA molecules. (**B**) AFM image from a M13 ssDNA + histone sample where monodisperse and globular nucleosome-like structures are observed. (**C**) Line scan along the red track in panel **B** indicating the measured height of histone-ssDNA complexes.

Fig. 6. Magnetic tweezers stretching and overwinding analysis of dsDNA and ssDNA. The single-molecule force-extension elasticity curves of (**A**) dsDNA and (**C**) ssDNA are fitted with WLC and extended WLC models, respectively (solid lines). Torsional unwinding curves under a preset force of 0.4 pN are shown for (**B**) dsDNA and (**D**) ssDNA. Error bars in panels **A** and **C** represent the standard deviation derived from four independent assays, each of them with a different individual molecule. The uncertainty of the end-to-end distance in panels **B** and **D** is in the range of 10 nm.

Fig. 7. MT stretching experiments of λ dsDNA and M13 ssDNA in the presence and absence of histones. (**A**) End-to-end distance shortening in the presence of 5 nM histone of a single λ dsDNA molecule held at a preset force of 0.5 pN. (**B**) Force-extension curves of M13 ssDNA in the absence (black, right) and in the presence of 10 nM histone (red, left). Solid lines show the extended WLC fit on the experimental data. (**C**) Typical real-time ssDNA extension measurement with a preset force of 15 pN. Black (upper), red (middle) and green (lower) solid lines exhibit the temporal extensions of M13 ssDNA in the presence of 0 nM, 10 nM and 500 nM histone, respectively; the three sets of data were obtained with the same individual molecule. Steps in the black line indicate the opening of ssDNA secondary structure. In panels **A** and **C** raw data are presented, whereas the error bars in panel **B** represent standard deviation derived from four independent experiments.

Fig. 8. Competitive association of core particle histones with M13 ssDNA and dsDNA. Samples containing both DNA species together were prepared in TE buffer supplemented with 0.15 M NaCl and analyzed in 1.4% agarose gels. Increasing amounts of histones were added to (**A**) a solution containing 52 µg/ml of each DNA form, and (**B**) to equimolar amounts of ssDNA and dsDNA (9.6 and 19.2 µg/ml respectively). (**C**) Linear regression representation of the titration with core histones of M13 ssDNA and dsDNA together in the same solution at the respective concentrations of 9.6 and 19.2 µg/ml. Mean values and standard deviations are derived from two independent replicas for each data point.

Fig. 9. Stability of histone-DNA aggregates. (**A**) M13 dsDNA (20 µg/ml) was complexed with histones (22 µg/ml) and titrated with increasing amounts of M13 ssDNA. Uncomplexed

dsDNA is shown in the first lane. (**B**) M13 ssDNA (9.2 µg/ml) was complexed with histones (22.1 µg/ml) and titrated with increasing amounts of M13 dsDNA. Uncomplexed ssDNA is shown in the first lane. Arrows indicate histone-DNA aggregates not entering the gel.

Fig. 10. Titration with histones of the different forms of NX1 fragment. Samples were prepared in TE buffer supplemented with 0.2 M NaCl, 6.6% sucrose, and an amount of BSA equal to the indicated histone content. Each lane contains 0.4 µg of NX1 dsDNA or 0.2 µg of NX1 ssDNA (+) or (–) strands. NX1 dsDNA was titrated with (**A**) core particle histones, (**B**) H3/H4, and (**C**) H2A/H2B. The electrophoretic mobility of native mononucleosomes (N) and dinucleosomes (diN) prepared from chicken erythrocyte nuclei is indicated as control. (**D**) Titration with core particle histones of NX1 ssDNA (–) and (+) strands. As controls are shown a sample containing 0.2 µg of each NX1 (+) and (–) strands and a lane containing 0.4 µg of NX1 dsDNA. (**E**) Titration of NX1 dsDNA and ssDNA(+) with the histone pairs H2A/H2B and H3/H4. The histone:DNA ratio is expressed as in Fig. 2.

Fig. 11. Scheme depicting the proposed interaction of ssDNA with core histones. (**A**) Hypothetical model consistent with the observed interaction of a fixed histone mass (here represented in orange as a core particle octamer) with equal lengths of dsDNA and ssDNA. (**B**) Cartoon showing a possible fate of nucleosomes in transcribed chromatin regions, where histones (red) would remain associated to noncoding ssDNA regions; coding ssDNA stretches are indicated in green.

Supplementary material

Biophysical characterization of the association of histones with single-stranded DNA

Ying Wang [a], Luis van Merwyk [a], Katja Tönsing [a], Volker Walhorn [a], Dario Anselmetti [a], Xavier Fernàndez-Busquets [b,c,d,*]

[a] Experimental Biophysics and Applied Nanoscience
Faculty of Physics, Bielefeld University
Bielefeld 33615, Germany

[b] Nanomalaria Group, Institute for Bioengineering of Catalonia (IBEC)
The Barcelona Institute of Science and Technology
Baldiri Reixac 10-12, Barcelona 08028, Spain

[c] Barcelona Institute for Global Health (ISGlobal)
Barcelona Center for International Health Research
(CRESIB, Hospital Clínic-Universitat de Barcelona)
Rosselló 149-153, Barcelona 08036, Spain

[d] Nanoscience and Nanotechnology Institute (IN2UB)
University of Barcelona
Martí i Franquès 1, Barcelona 08028, Spain

* Corresponding author.
E-mail address: xfernandez_busquets@ub.edu

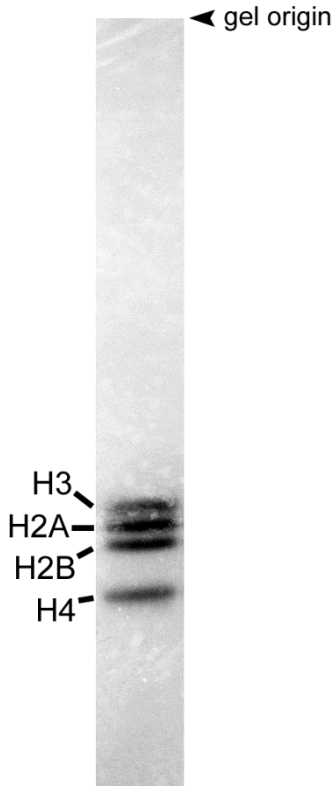

Supplementary Fig. 1. SDS-polyacrylamide gel electrophoresis analysis of a typical histone purification done in this work.

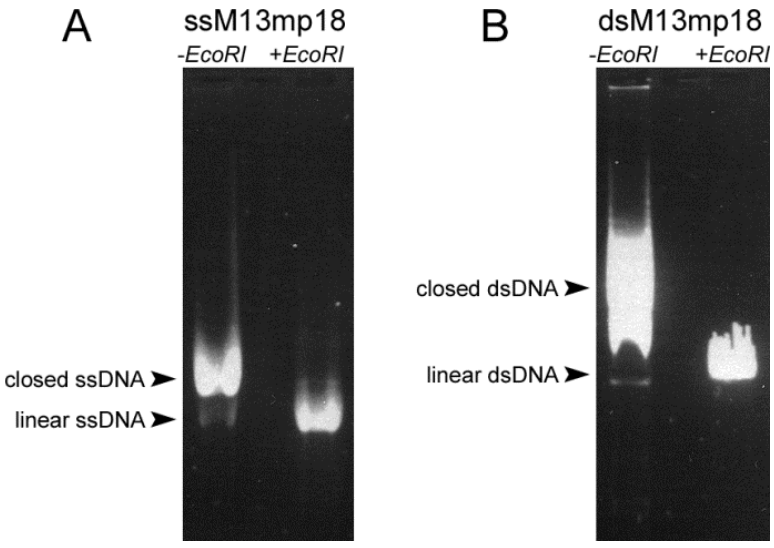

Supplementary Fig. 2. Analysis in 1.4% agarose gels of the linearization products of M13 (**A**) ssDNA and (**B**) dsDNA.

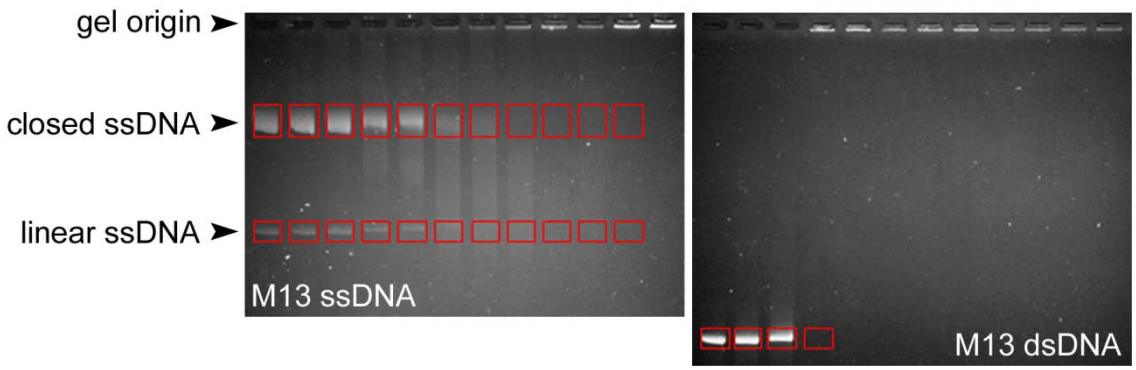

Supplementary Fig. 3. Quantification of the relative amounts of DNA in ethidium bromide-stained agarose gels. In an original negative where all DNA bands were below film saturation, the area occupied by the selected free DNA species (in the absence of histones, far left lane) was densitometered in all lanes at exactly the same distance from the gel origin. Red boxes indicate the scanned areas for the gels shown.

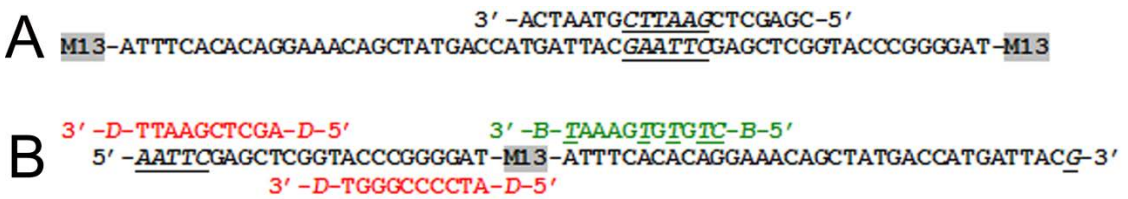

Supplementary Fig. 4. Scheme depicting (**A**) the strategy followed to linearize circular M13 ssDNA through *EcoRI* digestion and (**B**) the binding sites on the resulting linear DNA of (green, 3' end) biotinylated and (red, 5' end) digoxigenin-labeled oligonucleotides. B=biotin, C/T=dC/dT-biotin, D=digoxigenin.

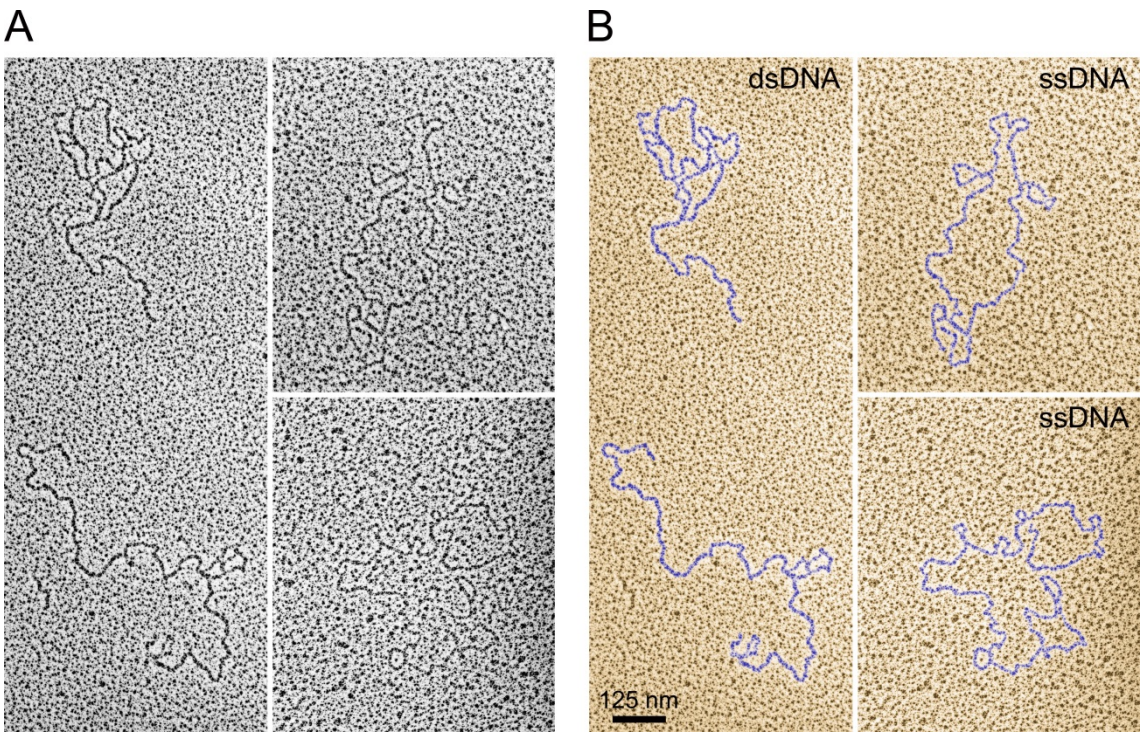

Supplementary Fig. 5. Analysis of the length of M13 ssDNA and dsDNA. Original TEM images of both DNAs (**A**) were artificially colored to highlight individual molecules (**B**). The respective estimated lengths were 2.35 ± 0.11 µm and 2.67 ± 0.44 µm for dsDNA and ssDNA, respectively. Molecule length was measured using the open source software package Easy Worm (Lamour et al., “Easyworm: an open-source software tool to determine the mechanical properties of worm-like chains”. Source Code for Biology and Medicine 2014, 9:16).

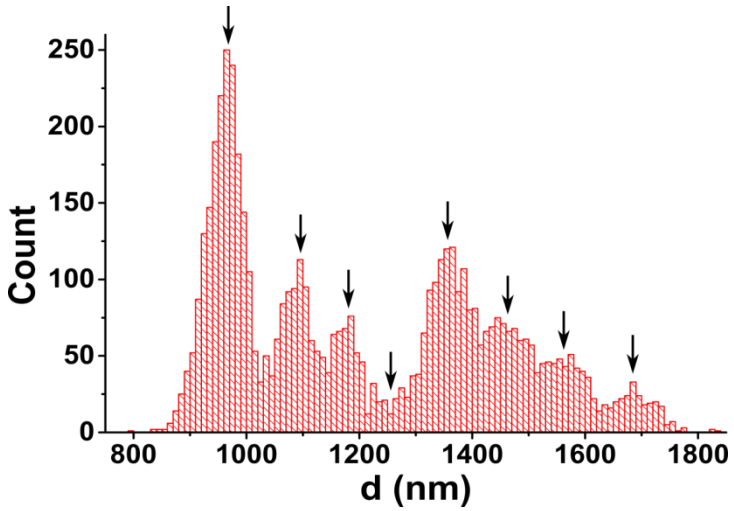

Supplementary Fig. 6. Histogram analysis of dsDNA end-to-end length decrease upon histone binding. Each end-to-end distance data point of a single histone binding experiment (Fig. 7A) is plotted in a histogram to identify plateaus of constant end-to-end distance between histone binding events. Arrows highlight the most probable dsDNA end-to-end distance of the corresponding plateaus. The fourth peak can hardly be discerned due to the short time interval between two subsequent binding events. The average distance between peaks was estimated to be ca. 102 nm.